Research papers

# Unsaturated flow effects on solute transport in porous media

Luwen Zhuang [a,b,c,*], Amir Raoof [c], Mojtaba G. Mahmoodlu [c,d], Sara Biekart [c], Riemer de Witte [c], Lubna Badi [c], Martinus Th. van Genuchten [c,e], Kairong Lin [a,b]

[a] School of Civil Engineering, Sun Yat-sen University, Zhuhai 519082, China
[b] Southern Marine Science and Engineering Guangdong Laboratory (Zhuhai), Zhuhai 519082, China
[c] Department of Earth Sciences, Utrecht University, P.O. Box 80021, 3508 TA Utrecht, Netherlands
[d] Department of Watershed and Rangeland Management, Gonbad Kavous University, Iran
[e] Center for Environmental Studies, São Paulo State University, UNESP, Rio Claro, SP 13506-900, Brazil

## ARTICLE INFO

## ABSTRACT

A major contaminant transport process in soils is hydrodynamic dispersion by affecting the spreading and arrival of surface-applied pollutants at underlying groundwater reservoirs. When a soil is unsaturated, hydrodynamic dispersion is very much affected by soil water saturation. Centimeter- and decimeter-scale column experiments were carried out to explore the effects of fluid saturation and particle size on the unsaturated solute dispersivity. Measured in-situ breakthrough curves were analyzed in terms of both classical advection–dispersion and dual-porosity (mobile-immobile) type transport equations. A clear non-monotonic relationship was found between the dispersivity and soil water saturation. The extent of non-monotonicity was more pronounced for a relatively coarse-textured sand compared to a finer sand. This finding has been reported rarely before; it explains some of the inconsistencies of saturation-dispersivity relationships in the literature.

## 1. Introduction

Contaminants released at or near the earth surface may travel through the soil unsaturated zone to arrive at and pollute underlying groundwater resources. Knowledge of the processes governing the fate and transport of pollutants in the unsaturated zone is a major aspect of risk assessments and remediation of contaminated aquifers (Bear and Alexander, 2010). Many studies have been carried out to investigate solute transport processes in the saturated zone (e.g., Fitch and Jia, 1996; Chiogna et al., 2010; Rolle et al., 2010; Gai et al., 2011). Soil texture and travel distance are well-known for influencing the dispersion process significantly. An additional complexity in the unsaturated (vadose) zone is the effect of soil water content (or fluid saturation) on solute dispersion (Bear, 1988), an issue that remains relatively ill-defined (Scheidegger, 1961; Yule and Gardner, 1978; Bolt, 1979; De Smedt et al., 1986; Gelhar, 1986). Several studies (e.g., Kirda et al., 1973; De Smedt et al., 1986; Maraqa et al., 1997; Matsubayashi et al., 1997; Devkota et al., 1998; Padilla et al., 1999; Kumahor et al., 2015) have shown an increase in the solute dispersivity for unsaturated soils compared to fully saturated conditions. Still other studies (Yule and Gardner, 1978; Costa and Prunty, 2006) found that dispersion remains

constant, regardless of the saturation level. A few recent laboratory-scale experimental studies (Bunsri et al., 2008; Toride et al., 2003; Karadimitriou et al., 2016) have shown a non-monotonic relationship between the solute dispersivity and soil water content, with the dispersivity increasing to a maximum value (referred to here as the maximum dispersivity) at some intermediate saturation and then decreasing with further desaturation. Raoof and Hassanizadeh (2013) could explain this non-monotonic dispersivity behavior based on a numerical study of pore-scale fluid flow and solute transport processes.

The laboratory studies referred to above were mostly conducted using repacked soil columns. More uncertainties are expected for field-scale undisturbed soils because of large-scale soil heterogeneity, soil layering, the presence of fractures and macropores, spatial variations in the flow velocity within the transport domain, time-dependent boundary conditions, root water uptake, and other complexities (e.g., Vanderborght et al., 2000, 2001; Javaux et al., 2006; Vanderborght and Vereecken, 2007; Koestel et al., 2009). Carefully constructed laboratory tracer experiments permit a far more precise assessment of the effects of soil moisture content on the dispersivity, as compared to field-scale situations. The discrepancies in the literature referred to above were likely due in part also to different soil types being used in the various

---

studies. Soil texture and soil structure affect water and air distributions at a given saturation, which in turn affects prevailing fluid velocity variations and solute mixing, resulting in different solute spreading and dispersion phenomena. Additionally, scale effects are important for solute dispersion (e.g., Dagan, 1986; Butters et al., 1989; Bromly and Hinz, 2004; Bromly et al., 2007; Mayer et al., 2008); however, their impact under unsaturated conditions remains unclear.

Another unsettled issue is the selection of an appropriate macro-scale model, which could be the classical equilibrium Advection-Dispersion Equation (ADE), a dual-porosity type Mobile-Immobile Model (MIM), or some other formulation. Some studies suggested the use of MIM type models (e.g., De Smet et al., 1981; Beven and Young, 1988; Geiger and Durnford, 2000), while others (e.g., Maraqa et al., 1997) show the suitability of the ADE to model transport without requiring immobile liquid zones. Still, the various transport models do need relationships for macroscopic coefficients related to solute dispersion and possible nonequilibrium mass transfer processes. Similar to the constitutive relationships for fluid flow, transport parameters are known to depend on pore structure as well as on actual air and water phase distributions. A lack of available constitutive data is often cited as a primary barrier to obtaining acceptable predictions (Toride et al., 2003).

Although advection and dispersion are generally considered to be the most important transport processes, there is ample evidence that solute diffusion into immobile or dead-end zones also affect solute residence times and resulting concentration distributions. Criteria are needed for choosing a particular macro-scale model that can be used for different soil types and fluid saturation scenarios, including variably-saturated conditions. Unfortunately, only a few well-controlled laboratory-scale hydrodynamic dispersion experiments exist for unsaturated flow conditions, especially experiments that consider a broad range of saturations. One major reason for this relates difficulties to establish uniform flow conditions at relatively low fluid saturations.

In this paper we present results of a systematic numerical and experimental study on solute transport under saturated and unsaturated conditions. Our aim is to investigate several factors influencing unsaturated transport, such as soil texture and the effects of scale. We performed a series of solute transport experiments for different sandy soils having a wide range of fluid saturations. Moreover, we employed two experimental setups with different column lengths to explore the scale dependency of unsaturated solute dispersion. Breakthrough curves (BTCs) were measured in situ at different points along the flow path. The equilibrium ADE and nonequilibrium-based MIM models were used to analyze the experimental data and to obtain solute dispersivities at different fluid saturations. The resulting dependency of the solute dispersivity on saturation is shown and discussed.

## 2. Materials and methods

### 2.1. Materials

Two different sands were used in the experiments. A relatively fine sand, S1, was obtained from a mining site in Belgium, and a coarse sand, S2, from a riverbed in the Netherlands. Before their use the sands were washed using deionized water to remove clay particles. Properties of the

two sands are listed in Table 1. The HYPROP evaporation device (UMS AG, Germany) was used to obtain soil water retention data of the two sands, and to find the corresponding van Genuchten (1980) soil hydraulic parameters. The resulting curves are shown in Fig. 1, while the optimized hydraulic parameter values are listed in Table 1. Compared with sand S1, the coarser sand S2 had a lower air entry pressure as reflected by a larger $\alpha$ value, and a larger value of residual water saturation.

### 2.2. Experimental apparatus and procedures

We employed a 37-cm long plexiglass column with an inner diameter of 10 cm to perform the unsaturated flow and solute transport experiments. The setup is shown in Fig. 2. Since the dispersivity is sensitive to possible nonuniformities of flow across the inlet boundary, we placed a paper filter on top of the column to uniformly distribute water over the entire inlet surface area. A 5-mm thick hydrophilic filter was used at the bottom of the column to serve as a capillary barrier preventing air penetration into the sample. A vacuum pump furthermore was used at the outlet to precisely control the outlet water pressure head.

The columns were packed by pouring dry sand into the water-filled columns. During packing, we regularly tapped the sands and scratched their surface to avoid layering. To ensure complete saturation, $CO_2$ was injected overnight before saturating the columns. Deionized and degassed water was used in all experiments. Several sensors were used for the required measurements. Three micro-tensiometers (Rhizo Instruments, Netherlands) were installed at depths of 10.5, 18.0, and 25.5 cm, respectively, to measure pressure heads along the samples. The tensiometers consisted of a ceramic cup having dimensions of 1 cm in length and 4 mm in diameter, as well as a small pressure transducer. We further inserted probes (5-TE sensors, Decagon Devices, USA) at the same depths to obtain the electrical conductivity, dielectric permittivity, and temperature simultaneously at those locations. This allowed us to also estimate water saturation of a given sample from the dielectric permittivity using the Topp empirical formula (Topp et al., 1980). When injecting a tracer solution, the solute concentration is linearly related to the electrical conductivity at a given value of water saturation (Toride et al., 2003). All data were collected using a CR1000 data logger (Campbell Scientific, UK).

Solute transport experiments were carried out under both saturated and unsaturated flow conditions. The saturated flow experiments involved two different flow rates. After establishing steady-state flow using solute-free water, a three-way valve was used to start injecting a $CaCl_2$ solution (0.08 mol/L) for a certain pore volume, and then returning to solute-free water to create a solute pulse. Concentration breakthrough curves (BTCs) were measured at three depths using the 5-
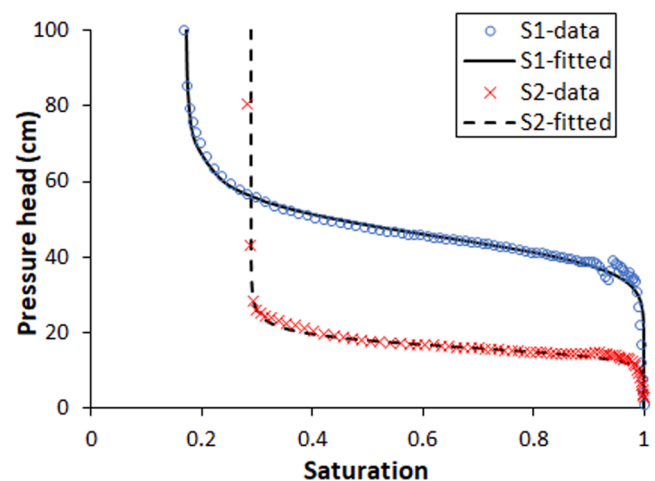
**Table 1**
Properties of sands S1 and S2 used in the experiments.

| Properties | S1 | S2 |
|---|---|---|
| Particle size (mm) | 0.1–0.5 | 0.3–0.8 |
| Mean particle diameter, $d_{50}$ (mm) | 0.20 | 0.50 |
| Uniformity coefficient, $d_{60}/d_{10}$ | 1.7 | 1.2 |
| van Genuchten parameter, $\alpha$ (cm$^{-1}$) | 0.022 | 0.062 |
| van Genuchten parameter, $n$ (-) | 10.0 | 10.0 |
| Residual water saturation, $S_r$ (-) | 0.17 | 0.29 |
| Saturated conductivity, $K_s$ (cm min$^{-1}$) | 1.02 | 4.80 |
| Average porosity, $\varphi$ (-) | 0.39 | 0.37 |



**Fig. 1.** Water retention data for fine sand S1 and coarse sand S2.
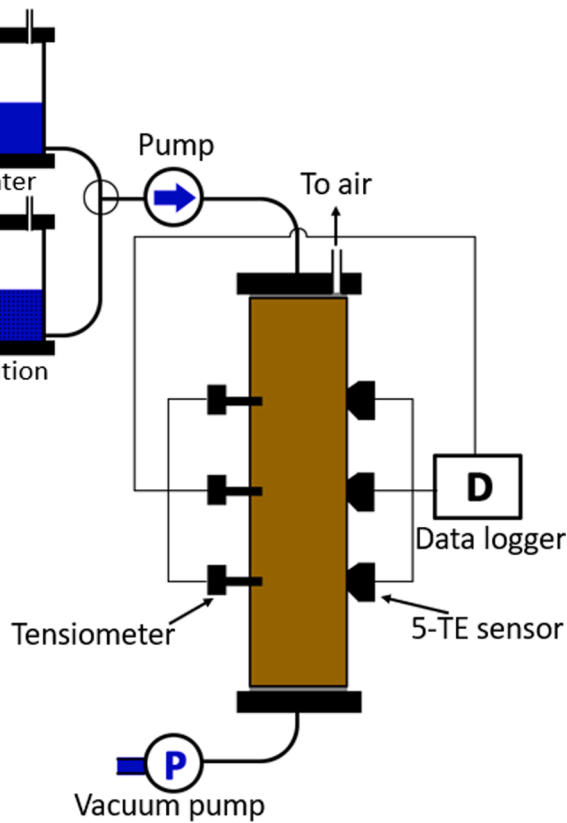
**Fig. 2.** Schematic view of the 37-cm long column.

TE sensors. For the transport experiments during unsaturated flow, unit-gradient flow conditions were established first before injecting the solute pulse at a given water saturation. This was done to obtain uniform water contents (i.e., no gradients in the capillary pressure) in the samples, which later allowed us to relate the observed solute dispersivity to a certain well-defined saturation value. To do so, starting from saturated flow conditions, the water inflow rate at the top and water pressure head at the bottom of the column were decreased gradually in order to minimize local hysteresis effects. The top of the column was open to air to keep the air pressure fixed at atmospheric level. During this process, we monitored the three tensiometers until they reached the same negative unsaturated pressure head, thus ensuring that unit gradient flow was achieved.

The solute dispersivity is known to be length-scale dependent. To investigate this effect at the laboratory scale, we performed, in addition to the experiments using 37-cm long sand columns, also transport experiments using a much smaller sample. The smaller sample had dimensions of 3 cm (height) by 3 cm (length) by 2 cm (width), filled with S1 sand. A schematic view of the small sandbox system is shown in Fig. 3. More details about the sample container can be found in Zhuang



**Fig. 3.** Schematic view of the 3-cm long sandbox system.

et al. (2017). For the smaller sample we used gamma ray transmission to measure water saturations and solute concentrations, thus avoiding the insertion of any physical sensors into the small sample. This avoided any disturbance of the soil, including possible gaps between the surface of the sensors and the soil particles. Measurement of the attenuation of gamma photons has been used often to determine the soil bulk density and water content, but not solute concentrations. For this study, we calibrated the attenuation to be able to also measure solute concentrations. Different solution concentrations lead to different attenuation intensities. The required relationship was based on calibration prior to the solute transport experiments. Detailed information about the gamma transmission method is given in the Supporting Information Text S1.

The transport experiments in the S1-sandbox under saturated flow conditions were carried out using two different water flow rates. For unsaturated flow conditions, a continuous flux was applied to the sand sample in the sandbox starting from primary drainage. After packing the saturated sand samples, we applied a flow rate slightly smaller than the measured saturated hydraulic conductivity (obtained with the constant-head method) to the top of the sample. The hanging water column was then kept at the same level as the bottom of the sand sample. Readings of the two tensiometers were monitored continuously. When readings of the two tensiometers were identical, water saturation of the sample was measured using the gamma ray system. The three-way valve subsequently was switched from solute-free water to a $CaCl_2$ solution for a certain number of pore volumes, and then switched back to solute-free water in order to create a solute pulse. The resulting concentration breakthrough curves (BTCs) were measured every 30 s using the gamma system.

In all we conducted eight experiments for sand S1 and ten experiments for sand S2 under variably-saturated flow conditions. The BTCs of the longer columns were observed at three depths for each experiment. For the small sample, we carried out eight experiments under both saturated and unsaturated flow conditions. The BTCs in the small column were measured at 1.5 cm from the inlet. Each experiment was carried out at least twice to validate the results.

### 2.3. Transport models

Since the solutes were injected uniformly across the entire inlet cross section, and the lateral boundaries were no-flow, overall macroscopic flow and solute transport in both setups can be considered to be one dimensional. The BTCs hence could be simulated using one-dimensional continuum scale modeling. Two different formulations were considered for this purpose: The classical Advection Dispersion Equation (ADE) and a dual-porosity type Mobile-Immobile model (MIM). We used the STANMOD software (Toride et al., 1995; Šimůnek et al., 1999) for all forward and inverse calculations.

For non-reactive solute transport such as in this study, the ADE is given by

$$\frac{\partial C}{\partial t} = D \frac{\partial^2 C}{\partial x^2} - v \frac{\partial C}{\partial x} \tag{1}$$

where $C$ represents the solute concentration, $v$ denotes the pore water velocity, $D$ is the hydrodynamic longitudinal dispersion coefficient, $t$ is time, and x is the spatial coordinate. The dispersivity $\lambda$ in the ADE formulation is defined as $\lambda = D/v$, thus implying that diffusion in our study had a negligible effect on longitudinal transport.

Nonequilibrium transport often exists during both saturated and unsaturated flow, leading to early arrival and tailing in observed BTCs (van Genuchten et al., 1977; De Smedt et al., 1986). One approach to account for this is to modify the ADE model to assume the presence of stagnant water in relatively small or dead-end pore spaces. MIM models consider total water saturation ($S$) to be made up of two regions: mobile water saturation ($S_m$) and immobile water saturation ($S_{im}$), with solute exchange between the two regions simulated as a first-order mass
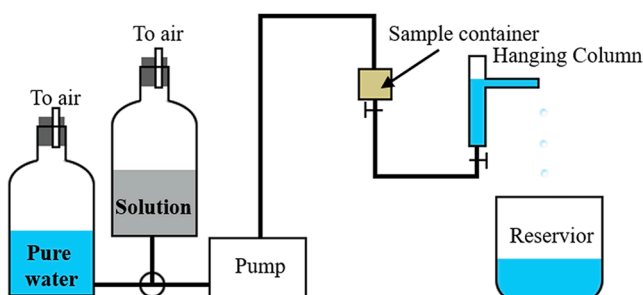
transfer process. The MIM model for non-reactive transport can be described as (Coats and Smith, 1964; van Genuchten et al., 1977)

$$S_m \frac{\partial C_m}{\partial t} + S_{im} \frac{\partial C_{im}}{\partial t} = S_m D_m \frac{\partial^2 C_m}{\partial x^2} - S_m v_m \frac{\partial C_m}{\partial x} \tag{2}$$

$$\varphi S_{im} \frac{\partial C_{im}}{\partial t} = \omega(C_m - C_{im}) \tag{3}$$

where the subscripts $m$ and $im$ refer to the mobile and immobile regions, respectively, $\varphi$ is the porosity, $\omega$ is the mass transfer coefficient between the mobile and immobile regions, and $v_m$ and $D_m$ are the pore water velocity and dispersion coefficient of the mobile liquid phase, respectively. We will use the parameter $\beta$ for the ratio of mobile saturation to total saturation (i.e., $\beta = S_m/S$), which implies that $v_m$ in Eq. (2) is related to $v$ through $v_m = v/\beta$, while further using $\lambda_m$ ($=D_m/v_m$) for the dispersivity in the MIM model.

We specified third-type inlet boundary conditions for both models, thus considering all concentration data to be volume-average variables (van Genuchten and Parker, 1984). The dispersion coefficient and the pore water velocity were the optimized parameters in the ADE model, while for the MIM model we also needed to optimize simultaneously the mass transfer coefficient $\omega$ and the mobile fluid ratio $\beta$ (in addition to $v_m$ and $D_m$). Optimizations were carried out in terms of the total resident concentration $C_T$ given by

$$C_T = C_m S_m + C_{im} S_{im} \tag{4}$$

## 3. Results and discussion

### 3.1. Breakthrough curves

We first present a selection of the BTCs that were measured at different locations and for different fluid saturations, as well their analysis in terms of the ADE and MIM models. Fitted values of the transport parameters are listed in Tables S1 to S12 of the Supporting Information. We note here that application of different macroscopic models (ADE and MIM in our case) will lead to different parameter values depending upon the formulation of the macroscopic equations.

Fig. 4 shows BTCs obtained under saturated flow conditions. Both fine sand S1 and coarse sand S2 provided symmetrical BTCs at all depths. Given the symmetry, the ADE model was sufficient to describe the data (the black solid lines in Fig. 4). By comparison, observed BTCs at intermediate saturation values, such as shown in Fig. 5 for $S = 0.44$, were less symmetrical with some tailing at both the higher and lower concentrations. This suggests the use of the MIM model in addition to the ADE. Results are shown in Fig. 5 as solid and dash lines, respectively.

The MIM model showed a slightly better description of the non-symmetric structure and tailing of the BTCs ($R^2$ values can be found in Tables S1-S12).

### 3.2. Dispersivities of the ADE and MIM models

#### 3.2.1. ADE model

Fig. 6 shows estimated dispersivity values as a function of water saturation using the ADE model. The results clearly indicate non-monotonic relationships between the solute dispersivity, $\lambda$, and saturation, $S$. The relatively fine sand (S1) column showed an increase in dispersivity as saturation decreased from 1.0 to 0.5, but then $\lambda$ slightly decreased when $S$ became less than 0.5. This behavior was consistent for all depths. Overall, $\lambda$ showed a slight non-monotonic behavior with a maximum value (the maximum dispersivity) at an intermediate saturation value of 0.5. We note that only one set of the BTCs was measured for saturations less than 0.5 for sand S1. This because of the very low permeability of the fine sand at low saturations, and hence the extremely long times needed to obtain complete BTCs. Coarse sand S2 showed far more visible non-monotonic behavior and a better defined maximum dispersivity (Fig. 6b). These results confirm that non-monotonicity exist in the dispersivity versus saturation, with the extent of non-monotonicity depending upon particle size (being less pronounced for our finer sand). Moreover, the $S$ value corresponding to the maximum dispersivity shifted to a relatively large value of around 0.6 for the coarse sand. Our results hence indicate that the changes in $\lambda$ with fluid desaturation depend upon soil texture, thus explaining some of the discrepancies about the unsaturated dispersivity reported in the literature. For instance, Toride et al. (2003) and Bunsri et al. (2008) showed non-monotonic relationships between $\lambda$ and fluid saturation for 0.25–0.50 mm and 0.15–0.5 mm sand particle sizes, which are slightly coarser than our sand S1. By comparison, Padilla et al. (1999) reported a more monotonic dispersivity-saturation relationship for their sand ranging from 0.05 to 0.43 mm (finer than our S1 sand). We emphasize here that the results of repacked laboratory column experiments may differ markedly from those of undisturbed soils and/or field situations. Many other uncertainties for field-scale undisturbed soils exist, such as large-scale heterogeneities, soil layering, fractures and macropores, spatial moisture variations along the transport domain, near-surface hydrophobicity, root water uptake, time-dependent soil surface boundary conditions, and other complexities. For these reasons one must be careful when comparing laboratory results for steady-state flow conditions using from repacked coarse-textured soils directly with field-scale observations.

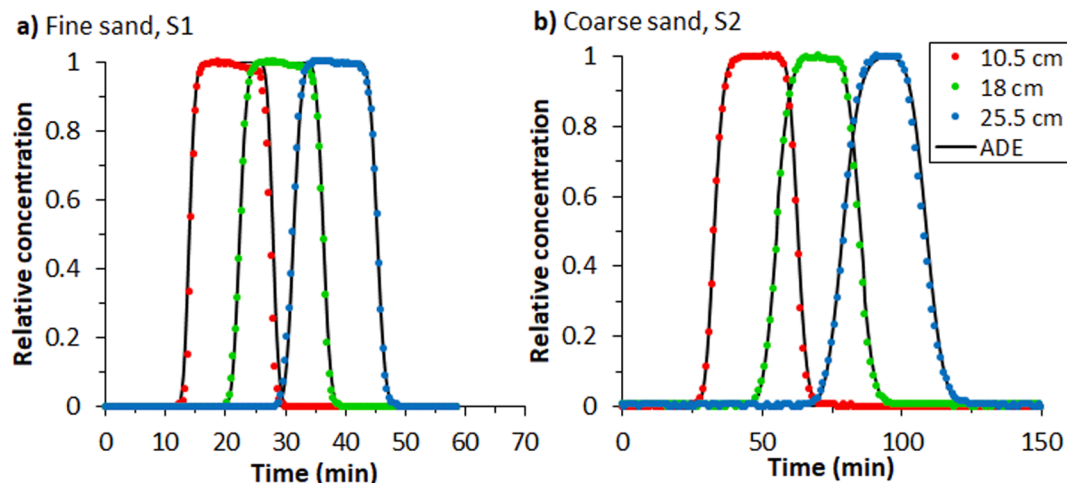At a given saturation level, the dispersivity changed with distance



**Fig. 4.** Saturated flow conditions: Observed and simulated BTCs for fine sand S1 and coarse sand S2.
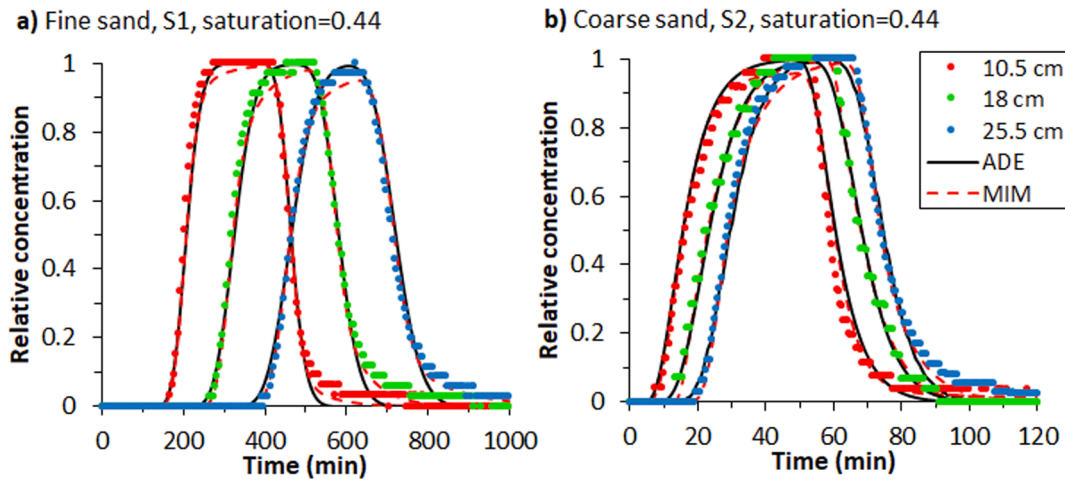
**Fig. 5.** Unsaturated flow conditions: Observed and simulated BTCs, at $S = 0.44$, for fine sand S1 and coarse sand S2.
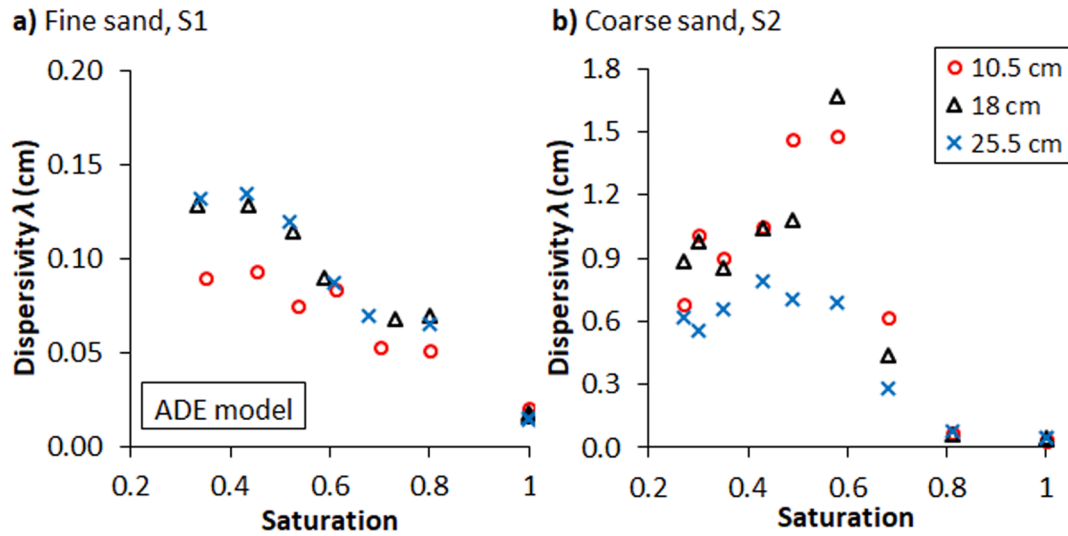


**Fig. 6.** ADE model results: dispersivity, $\lambda$, versus water saturation, S. at different depths for fine sand S1 (a), and coarse sand S2 (b).

due to its scale dependency. Our results showed an increase in the dispersivity up to a distance of 18.0 cm, where it reached an asymptotic value for sand S1. The accuracy of measurements close to the bottom (i. e., at 25.5 cm) may have been affected by hysteresis in the unsaturated hydraulic properties. The coarser sand, S2, was found to be less sensitive to the length scale. To further explore this effect, we used a non-destructive method (to prevent sample disturbance) to collect

dispersivity data for fine sand, S1.

### 3.2.2. MIM model

Changes in the dispersivity obtained with the MIM model (i.e., for the mobile phase dispersivity, $\lambda_m$) as a function of water saturation for both sands are shown in Fig. 7a. The transport parameters were obtained using the BTCs at the central location (i.e., at 18.0 cm) since those are
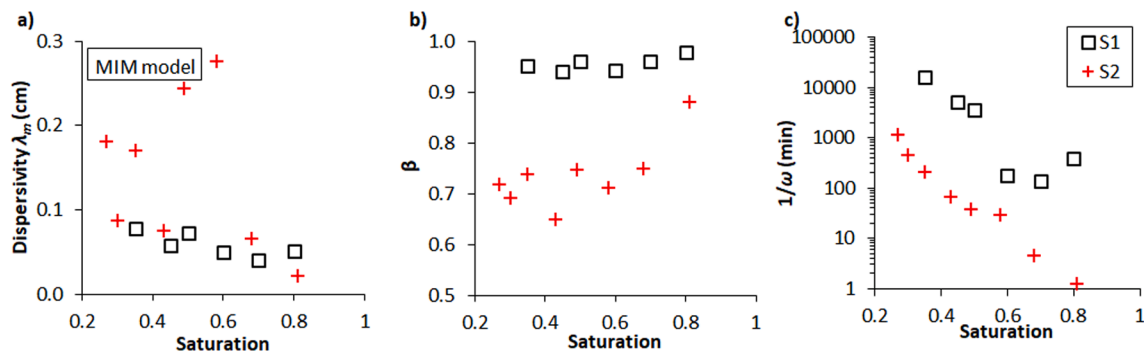


**Fig. 7.** Changes in solute transport parameters with saturation using the MIM model: variations in a) solute dispersivity of the mobile phase, $\lambda_m$, b) the mobile phase fraction, $\beta = S_m/S$, and c) the mass transfer equivalent time between the mobile and immobile phases, $1/\omega$.

affected the least by the inlet and outlet boundaries. The relationship between $\lambda_m$ and water saturation for coarse sand S2 showed a non-monotonic relation, similar as for the ADE model. However, the MIM values of $\lambda_m$ were six times smaller than the ADE $\lambda$ values.

Mass exchange between the mobile and immobile liquid phases is influenced by the relative amount of these phases and the mass transfer coefficient associated with this exchange. Fig. 7b presents the ratio ($\beta$) between mobile water saturation ($S_m$) and total saturation ($S$). The mobile water fraction was at its maximum during saturated conditions, but decreased as more air occupied the soil pores at lower saturation values (Griffioen et al., 1998). For fine sand S1, $\beta$ values decreased slightly and then remained nearly constant at a value of 0.96 as $S$ further decreased. For coarse sand S2, $\beta$ values decreased significantly at first, but then stayed at around 0.7 with further desaturation. Differences in the pore size and flow pathways between the two sands are the main causes of these differences in $\beta$. Sand S1 is a relatively fine to medium sand with relatively small pores and many connected flow pathways at a given saturation, while sand S2 is coarser with much larger pores and fewer connected pathways. Sand S2 with its fewer connected flow pathways was expected to show more immobile water.

Fig. 7c shows the mass transfer equivalent time, $1/\omega$, as a function of saturation under unsaturated flow conditions. For fine sand S1, when $S > 0.6$, the transfer time was very small, implying rapid solute exchange, while the transfer time increased dramatically by two orders of magnitude or more when $S < 0.6$, which qualitatively is consisted with conclusions by Griffioen et al. (1998). For coarse sand S2, the transfer time was relatively small over the entire saturation range, with a slight increase only when $S < 0.3$. Mass transfer hence required far less time for coarser sand S2 compared to finer sand S1.

We calculated the overall effective dispersivity also in terms of the MIM parameters. This parameter can be defined as follows (Valocchi, 1985; Toride et al., 2003):

$$\lambda_{MIM} = \lambda_m + \frac{S_{im}^2 S_m \varphi v_m}{\omega S^2} \tag{5}$$

where $\lambda_{MIM}$ is the overall effective MIM dispersivity, which accounts for dispersion in the mobile phase as well includes the effects of solute exchange between the mobile and immobile phases, and where $S_m$ and $S_{im}$ and are mobile and immobile saturations respectively.

The values of $\lambda_{MIM}$, $\lambda$, and $\lambda_m$ for the two sands are shown in Fig. 8. Values of $\lambda_m$ were always much smaller than those of $\lambda$ over the entire saturation range. This was to be expected since dispersion in the MIM formulation is represented using three parameters (i.e., by dispersivity

as such, as well by solute mixing between the mobile and immobile phases as predicated by the fraction mobile liquid $\beta$ ($=S_m/S$) and the mass transfer coefficient $\omega$), while in the ADE all of the mixing processes are lumped into a single dispersivity parameter $\lambda$. The $\lambda_{MIM}$ values for sand S1 were slightly larger than those of $\lambda$ over the entire saturation range, especially at the lower saturations, while the values of $\lambda_{MIM}$ and $\lambda$ were almost the same for sand S2.

### 3.3. Dispersivity at different scales

The above experiments were carried out using 37-cm long columns. We additionally used a very short 3-cm column to perform transport experiments for fine sand, S1. The resulting parameter values for the short column are listed in Table S13. Selected BTCs under saturated and unsaturated flow conditions are shown in Fig. 9. The BTCs exhibited some scattering in the concentration values, most likely due to local flow variations (the measurement area normal to the gamma ray flux was only 6 mm in diameter) and subsequent dynamic changes in the air-–water interfaces during gamma ray passage. We acknowledge here that BTCs from very short columns inherently are affected more by experimental imperfections associated with packing and the implementation of boundary conditions.

Fig. 10a shows a plot of normalized dispersivity values (relative to saturated $\lambda$ values) obtained using both the small 3-cm sample, as well as the larger 37-cm columns. Shown are data for the point closest to the inlet of the longer column (i.e., at 10.5 cm), which possibly may have been affected still slightly by the input boundary. The inset provides a view with a smaller scale of the $y$ axis. As saturation decreased, $\lambda$ values obtained with the small sample for fine sand S1 increased to around 0.6 cm at $S = 0.5$, and then decreased slightly, hence again showing a non-monotonic relationship. By comparison, the dispersivities obtained for coarse sand S2 were much more non-monotonic. Still, all of the samples with their different soil textures and sample lengths confirmed a saturation dependency of the solute dispersivity, with the dependency being far more pronounced and non-monotonic for the coarser sand (Fig. 10a). For the finer sand, for which we performed experiments with two different sample lengths, saturation had much more effect on the dispersivity of the longer column, but with the non-monotonicity being far less as compared to the coarser sand. Fluid saturation at the turning point (the critical saturation, $S_c$) was slightly lower for fine sand S1 ($S_c = 0.5$) compared to the coarse sand S2 ($S_c = 0.6$).

Interestingly, the results in Fig. 10a show a similar trend as found in previous studies where 3D pore-scale modeling was used to explore the
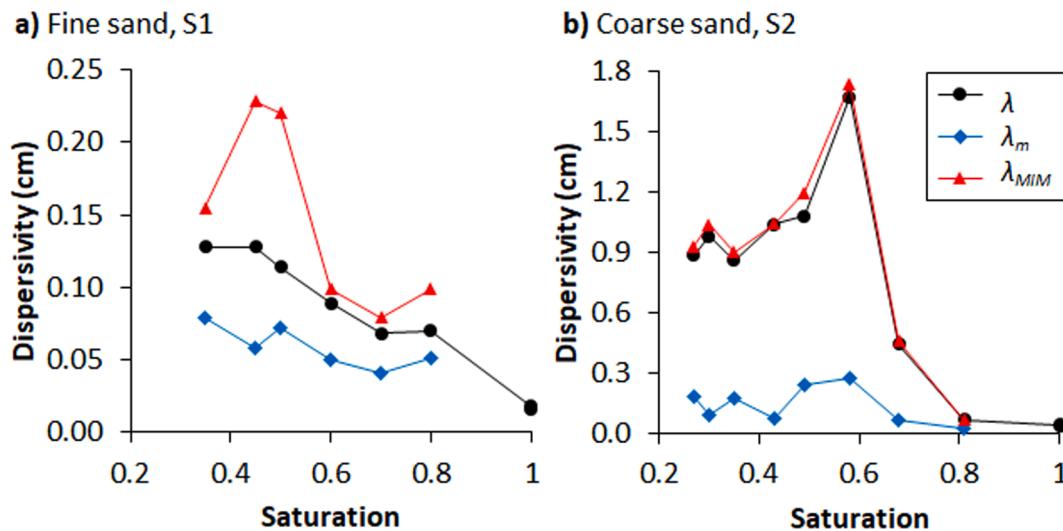


**Fig. 8.** Comparison between the effective overall dispersivity $\lambda_{MIM}$ as calculated with Eq. (5), $\lambda$ in the ADE model, and $\lambda_m$ in the MIM model for fine sand S1 (a), and coarse sand S2 (b).
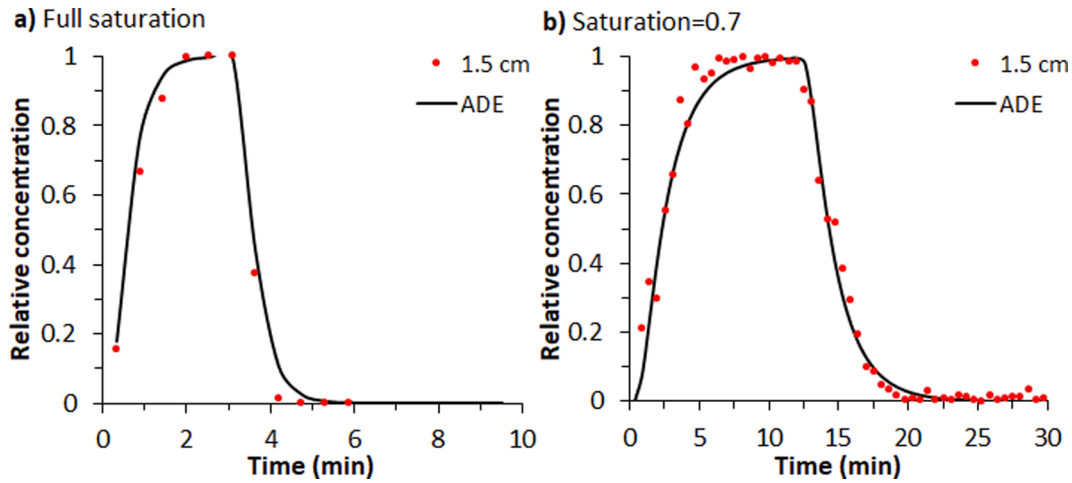
**Fig. 9.** Saturated and unsaturated flow conditions: Observed and simulated BTCs for fine sand S1 using the 3-cm sandbox.
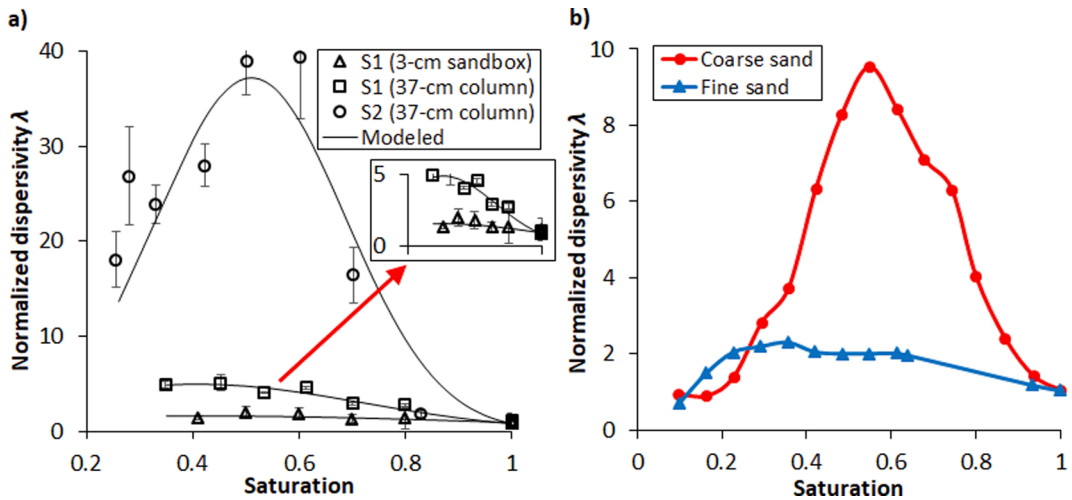


**Fig. 10.** a) Comparison of normalized dispersivity values, $\lambda$, using the ADE model for both sands, as well as for different sample sizes for sand S1, and b) relationships between the normalized dispersivity $\lambda$ and saturation as reported by Raoof and Hassanizadeh (2013) based on 3D pore-scale network modeling of samples with different pore sizes. Values of $\lambda$ in a) for the larger columns were for the BTCs at 10.5 cm (closest to the inlet of the columns); solid lines show the fitted relationships to the data.

saturation dependency of the dispersivity using samples with different pore size distributions (Fig. 10b, Raoof and Hassanizadeh, 2013). Consistent with that study, the experimental observations can be explained by the underlying pore scale processes. For unsaturated conditions, $\lambda$ is affected by the amount of mixing at the level of individual pores, which becomes limited due to the presence of air in the larger pores. Furthermore, at the level of sample size, dispersivity is affected by pore connectivities and whether in an unsaturated soil a cluster of connected saturated pores exist to form a flow pathway that percolates though the entire sample. Sand S2 having larger pores as reflected also by its capillary pressure–saturation curve showed the much higher dispersivity values. For this sand, air during drainage enters larger pores and effectively disconnects them from the otherwise still connected saturated pore system that forms fast flow pathways through the soil. Eliminating these fast pathways causes velocity variations to become less among different parts of the sample and, therefore, causes $\lambda$ to decrease. Raoof and Hassanizadeh (2013) showed that this dispersivity turning point ($\lambda_c$) occurs at higher saturation values for soils having larger pore sizes, consistent with our observations (Fig. 10). For a soil with smaller pore sizes (e.g., sand S1) the effect of the pathways and their elimination by the invading air phase become less distinct, which is also supported by the pore-scale network studies. For such a sample, the

turning point of the dispersivity occurs at lower saturations, while changes in $\lambda$ are affected less by saturation compared with samples having larger pore sizes.

To describe the relationship between the normalized dispersivity and saturation explicitly, we propose an empirical formula with a Gaussian shape as follows

$$\lambda(S) = ae^{-\left(\frac{S-b}{c}\right)^2}$$

(6)

in which $a$, $b$, and $c$ are fitting parameters, and $\lambda(S)$ is the normalized dispersivity. We applied Eq. (6) to the three sets of $\lambda$-$S$ data. The resulting curves are shown as solid lines in Fig. 10a, while the parameter values are given in Table 2. The values of $a$ and $b$ were close to the

**Table 2**
Values of the parameters $a$, $b$ and $c$ in Eq. (6) for sands S1 and S2.

| Experiment | A | b | c |
|---|---|---|---|
| S1-sandbox | 1.50 | 0.41 | 0.81 |
| S1-column | 4.91 | 0.45 | 0.39 |
| S2-column | 37.2 | 0.49 | 0.24 |

maximum dispersivity and the critical saturation, respectively. Knowing the maximum dispersivity and the critical saturation, it is then possible to predict $\lambda$ over the entire saturation range (especially saturation levels larger than residual saturation). Relationships such as those given by Eq. (6) may well become useful for field-scale modeling of solute transport in the unsaturated zone.

## 4. Conclusions

This study provides a comprehensive analysis of solute transport for two different sandy soils under saturated and a wide range of unsaturated flow conditions. Results showed a well-defined dependence of the solute dispersivity on soil water saturation, with the resulting relationship being non-monotonic, particularly for the coarser medium. The established relationship between solute dispersivity and water saturation may prove to be useful for field-scale contaminant transport models of the unsaturated zone to provide a better basis for subsurface environmental management and risk analyses. Our study involved carefully packed homogeneous fine and coarse sands. Further studies are clearly needed for different natural soils, especially structured or macroporous field soils, to test and/or improve the suggested relationship between the solute dispersivity and water saturation in the unsaturated zone.

## CRediT authorship contribution statement

**Luwen Zhuang:** Methodology, Software, Validation, Writing - original draft. **Amir Raoof:** Conceptualization, Supervision, Writing - review & editing, Funding acquisition. **Mojtaba G. Mahmoodlu:** Methodology, Supervision. **Sara Biekart:** Investigation. **Riemer de Witte:** Investigation. **Lubna Badi:** Investigation. **Martinus Th. van Genuchten:** Supervision, Writing - review & editing. **Kairong Lin:** Writing - review & editing.

## Declaration of Competing Interest

The authors declare that they have no known competing financial interests or personal relationships that could have appeared to influence the work reported in this paper.

## Acknowledgments

## Appendix A. Supplementary data

Supplementary data to this article can be found online at https://doi.org/10.1016/j.jhydrol.2021.126301.

## References

Bear, J., 1988. Dynamics of Fluids in Porous Media. Dover, New York.

Bear, J., Alexander, H.D.C., 2010. Modeling Groundwater Flow and Contaminant Transport. Springer, Dordrecht.

Beven, K.J., Young, P.C., 1988. An aggregated mixing zone model of solute transport through porous media. J. Contam. Hydrol. 3, 129–143.

Bolt, G.H., 1979. Movement of solutes in soil: principles of adsorption/exchange chromatography. Dev. Soil 5, 285–348.

Bromly, M., Hinz, C., 2004. Non-Fickian transport in homogeneous unsaturated repacked sand. Water Resour. Res. 40, W07402.

Bromly, M., Hinz, C., Aylmore, L.A.G., 2007. Relation of dispersivity to properties of homogeneous saturated repacked soil columns. Eur. J. Soil Sci. 58, 293–301.

Bunsri, T., Sivakumar, M., Hagare, D., 2008. Influence of dispersion on transport of tracer through unsaturated porous media. J. Appl. Fluid Mech. 1, 37–44.

Butters, G.L., Jury, W.A., Ernst, F.F., 1989. Field scale transport of bromide in an unsaturated soil: 1. Experimental methodology and results. Water Resour. Res. 25, 1575–1581.

Chiogna, G., Eberhardt, C., Grathwohl, P., Cirpka, O.A., Rolle, M., 2010. Evidence of compound-dependent hydrodynamic and mechanical transverse dispersion by multitracer laboratory experiments. Environ. Sci. Technol. 44, 688–693.

Coats, K.H., Smith, B.D., 1964. Dead-end pore volume and dispersion in Porous Media. Soc. Pet. Eng. J. 4, 73–84.

Costa, J.L., Prunty, L., 2006. Solute transport in fine sandy loam soil under different flow rates. Agric. Water Manag. 83, 111–118.

Dagan, G., 1986. Statistical theory of groundwater flow and transport: pore to laboratory, laboratory to formation, and formation to regional scale. Water Resour. Res. 22, 120S–134S.

De Smedt, F., Wauters, F., Sevilla, J., 1986. Study of tracer movement through unsaturated sand. J. Hydrol. 85, 169–181.

Devkota, L., Matsubayashi, U., Takagi, F., 1998. A new form of dispersion coefficient model for the porous media. Annu. J. Hydraul. Eng. 42, 355–360.

Fitch, A., Jia, D.U., 1996. Solute transport in clay media: Effect of humic acid. Environ. Sci. Technol. 30, 12–15.

Gai, K., Shi, B., Yan, X., Wang, D., 2011. Effect of dispersion on adsorption of atrazine by aqueous suspensions of fullerenes. Environ. Sci. Technol. 45, 5959–5965.

Geiger, S.L., Durnford, D.S., 2000. Infiltration in homogeneous sands and a mechanistic model of unstable flow. Soil Sci. Soc. Am. J. 64, 460–469.

Gelhar, L.W., 1986. Stochastic subsurface hydrology from theory to applications. Water Resour. Res. 22, 135S–145S.

Griffioen, J.W., Barry, D.A., Parlange, J.Y., 1998. Interpretation of two-region model parameters. Water Resour. Res. 34 (3), 373–384.

Javaux, M., Vanderborght, J., Kasteel, R., Vanclooster, M., 2006. Three-dimensional modeling of the scale- and flow rate-dependency of dispersion in a heterogeneous unsaturated sandy monolith. Vadose Zone J. 5 (2), 515–528.

Karadimitriou, N.K., Joekar-Niasar, V., Babaei, M., Shore, C.A., 2016. Critical role of the immobile zone in Non-Fickian two-phase transport: a New Paradigm. Environ. Sci. Technol. 50, 4384–4392.

Kirda, C., Nielsen, D.R., Biggar, J.W., 1973. Simultaneous transport of chloride and water during infiltration. Soil Sci. Soc. Am. Proc. 37, 339–345.

Koestel, J., Vanderborght, J., Javaux, M., Kemna, A., Binley, A., Vereecken, H., 2009. Noninvasive 3-D transport characterization in a sandy soil using ERT: 1. investigating the validity of ERT-derived transport parameters. Vadose Zone J. 8 (3), 711–722.

Kumahor, S.K., de Rooij, G.H., Schlüter, S., Vogel, H.-J., 2015. Water flow and solute transport in unsaturated sand—A comprehensive experimental approach. Vadose Zone J. 14.

Maraqa, M.A., Wallace, R.B., Voice, T.C., 1997. Effects of degree of water saturation on dispersivity and immobile water in sandy soil columns. J. Contam. Hydrol. 25, 199–218.

Matsubayashi, U., Devkota, L.P., Takagi, F., 1997. Characteristics of the dispersion coefficient in miscible displacement through a glass beads medium. J. Hydrol. 192, 51–64.

Mayer, A., Sandman, T., Breidenbach, M., 2008. Effect of flow regime on physical nonequilibrium transport in unsaturated porous media. Vadose Zone J. 7, 981–991.

Padilla, I.Y., Yeh, T.-C.-J., Conklin, M.H., 1999. The effect of water content on solute transport in unsaturated porous media. Water Resour. Res. 35, 3303–3313.

Raoof, A., Hassanizadeh, S.M., 2013. Saturation-dependent solute dispersivity in porous media: pore-scale processes. Water Resour. Res. 49, 1943–1951.

Rolle, M., Chiogna, G., Bauer, R., Griebler, C., Grathwohl, P., 2010. Isotopic fractionation by transverse dispersion: flow-through microcosms and reactive transport modeling study. Environ. Sci. Technol. 44, 6167–6173.

Scheidegger, A.E., 1961. General theory of dispersion in porous media. J. Geophys. Res. 66, 3273–3278.

Simunek, J., van Genuchten, M.T., Sejna, M., Toride, N., Leij, F.J., 1999. The STANMOD computer program for evaluating solute transport in porous media using analytical solutions of convection-dispersion equation. IGWMC-TPS-71, International Ground Water Modeling Center, Colorado School of Mines, Golden, Colorado, 32p.

Smet, F. de, Wierenga, P.J., Beken, A., 1981. Theoretical and experimental study of solute movement through porous media with mobile and immobile water. VUB Hydrol. 6, V.U.B., Brussel, Belgium.

Topp, G.C., Davis, J.L., Annan, A.P., 1980. Electromagnetic determination of soil water content: Measruements in coaxial transmission lines. Water Resour. Res. 16, 574–582.

Toride, N., Inoue, M., Leij, F.J., 2003. Hydrodynamic dispersion in an unsaturated dune sand. Soil Sci. Soc. Am. J. 67, 703–712.

Toride, N., Leij, F.J., van Genuchten, M.Th., 1995. The CXTFIT code for estimating transport parameters from laboratory or field tracer experiments. U.S. Salinity Laboratory Res. Rep. 137, U.S. Salinity, Riverside, CA.

Valocchi, A.J., 1985. Validity of the local equilibrium assumption for modeling sorbing solute transport through homogeneous soils. Water Resour. Res. 21 (6), 808–820.

van Genuchten, M.T., 1980. A closed-form equation for predicting the hydraulic conductivity of unsaturated soils. Soil Sci. Soc. Am. J. 44, 892–898.

van Genuchten, M.T., Parker, J.C., 1984. Boundary conditions for displacement experiments through short laboratory soil columns. Soil Sci. Soc. Am. J. 48, 703–708.

van Genuchten, M.T., Wierenga, P.J., O'Connor, G.A., 1977. Mass transfer studies in sorbing porous media: III. Experimental evaluation with 2,4,5-T. Soil Sci. Soc. Am. J. 41, 278–285.

Vanderborght, J., Timmerman, A., Feyen, J., 2000. Solute transport for steady-state and transient flow in soils with and without macropores. Soil Sci. Soc. Am. J. 64 (4), 1305–1317.

Vanderborght, J., Vanclooster, M., Timmerman, A., Seuntjens, P., Mallants, D., Kim, D.J., Jacques, D., Hubrechts, L., Gonzalez, C., Feyen, J., Diels, J., Deckers, J., 2001. Overview of inert tracer experiments in key Belgian soil types: relation between transport and soil morphological and hydraulic properties. Water Resour. Res. 37 (12), 2873–2888.

Vanderborght, J., Vereecken, H., 2007. Review of dispersivities for transport modeling in soils. Vadose Zone J. 6, 29–52.

Yule, D.F., Gardner, W.R., 1978. Longitudinal and transverse dispersion coefficients in unsaturated plainfield sand. Water Resour. Res. 14, 582–588.

Zhuang, L., Bezerra Coelho, C.R., Hassanizadeh, S.M., van Genuchten, M.T., 2017. Analysis of the hysteretic hydraulic properties of unsaturated soil. Vadose Zone J. 16, 9p.